Geometric constraints on energy transfer in the turbulent cascade

Joseph G. Ballouz and Nicholas T. Ouellette*
Department of Civil and Environmental Engineering, Stanford University, Stanford, California 94305, USA

(Received 9 September 2019; accepted 18 February 2020; published 11 March 2020)

The energy cascade is the most significant feature that separates turbulence from other unsteady flows, and results from the behavior of the nonlinear term in the Navier-Stokes equations. The mathematical form of this term, however, places constraints on exactly how it can act. Here we consider the action of the nonlinear term in physical space rather than in Fourier space, where the energy transfer between scales can be interpreted as a mechanical process where some scales do work on others. This formulation reveals the fundamental role played by geometry, as work can only be done when the eigenframes of the turbulent stress and strain rate are appropriately aligned. By comparing a direct numerical simulation of the Navier-Stokes equations, an ensemble of random solenoidal vector fields, and a random sampling of uniform eigenframe alignments, we show that this geometric alignment plays a much stronger role in determining the flux between scales than do the magnitudes of the stress and strain rate. We also show that when the alignment is effectively two dimensional, even when embedded in a three-dimensional flow, the energy flux is typically inverse, suggesting that the inverse cascade in two-dimensional turbulence may have a kinematic origin. Our results point to some potentially fruitful directions for turbulence modeling.

DOI: 10.1103/PhysRevFluids.5.034603

I. INTRODUCTION

Nonlinearity is common in fluid mechanics as well as in complex systems more broadly, with consequences ranging from unpredictable chaotic dynamics to the emergence of coherent structures. The most salient effect of nonlinearity that distinguishes turbulence from more generic unsteady flows is the cascade of energy from the scales at which it is injected into the flow to the scales at which it is dissipated. Appropriately accounting for this cascade process is thus a key goal in turbulence modeling, ideally with the result of being able to capture the outcome of the cascade without explicitly representing all scales. Statistical models of the cascade, going back to the pioneering work of Kolmogorov [1] with more recent refinements such as multifractality [2–4], have had success in describing some aspects of the cascade, but still struggle to completely capture effects such as intermittency [5,6]. Fully statistical pictures may also hide the underlying physical mechanisms that drive the cascade, making it difficult to see what aspects of the model ought to be modified on physical grounds.

To attempt to remedy this situation, any number of physical mechanisms for the cascade have been proposed over the years. The most persistent go back to Taylor [7–9] and suggest that vortex stretching is the fundamental ingredient that drives the transfer of energy from large to small scales in three-dimensional (3D) turbulence. This phenomenology considers turbulence to be an ensemble of vortex tubes embedded in a strain field. Due to vortex tilting and stretching, these tubes are imagined to align locally with the extensional directions of the strain field, at which point they are

*nto@stanford.edu

stretched. Conservation of angular momentum then suggests that the vorticity of the tubes should be increased while their diameters shrink, thereby energizing smaller and smaller scales of motion until they are finally small enough that viscous forces can dissipate the energy [10].

With the rise of high-Reynolds-number direct numerical simulation (DNS) and precision experimental measurements, however, many of the assumptions of this phenomenology have been challenged. The notion that vortex stretching drives the cascade suggests that, on average, the vorticity vector ought to be aligned with the most extensional eigenvector of the strain rate. However, while there is a tendency toward this alignment when viewed in an appropriate Lagrangian setting [10,11], there is little instantaneous alignment between the vorticity and the extensional strain [12–16]. There is increasing skepticism about the dynamical relevance of concentrated vorticity in turbulence [17], and recent mathematical results have provided strong arguments against vortex stretching as the dynamical mechanism responsible for the cascade [18]. The case of 2D turbulence, where the energy cascade reverses direction and transports energy to scales larger than the injection scale, also presents a different kind of challenge to the notion of a vorticity-driven cascade. Vortex stretching is geometrically forbidden in 2D Navier-Stokes systems and so clearly cannot be the mechanism responsible for the inverse cascade. Thus, even though a conceptually similar cascade still exists in two dimensions, its physical mechanism would have to be wholly distinct from the 3D case if the mechanism for the 3D cascade were indeed vortex stretching. While it is certainly possible that the 2D and 3D situations could simply be different, it would be more appealing to be able to find similarities between the two.

To gain a fresh perspective on the cascade, we consider it not in Fourier space, as is typically done, but rather in physical space [15,19] and treat it as a mechanical process [20,21]. In contrast to vorticity-based phenomenologies, this reframing allows us to make a direct connection between a physical picture of the flow and the term in the equations of motion that drives energy between scales. The key quantity in the equations of motion is the inner product between the turbulent stress and strain-rate tensors, as we show below. When the eigenframes of these tensors are well aligned, energy is transferred between scales, but when they are misaligned, the scale-to-scale energy flux is suppressed. As we have reported previously, these tensors tend to be surprisingly poorly aligned in turbulence, with the implication that much less energy is actually transferred through the cascade than would be theoretically possible. These results hold in both 3D [21] and 2D turbulence [22], suggesting a possible dynamical similarity between the two cases.

Here we study the degree to which these fundamentally geometric properties are driven by the turbulence dynamics (that is, the specific equations of motion that determine the evolution of the flow) as compared with the constraints imposed on them by the mathematical form of the energy transfer term in the Navier-Stokes equations and the embedding dimension. To do so, we compare three kinds of numerical data: a DNS of Navier-Stokes turbulence, a random, multiscale solenoidal vector field (akin to those used in so-called kinematic simulations [23]), and uniform Monte Carlo sampling of the space of possible geometric alignments between two tensors. Our results indicate that many of the properties of the cascade are indeed kinematic, in that they are reproduced without Navier-Stokes dynamics. We find that although the magnitudes of these tensors depend on the dynamics, the efficiency of the scale-to-scale energy transfer (that is, the ratio of the amount of energy actually transferred between scales to the maximum possible amount) is set almost entirely by the tensor alignment. The flow dynamics do control the statistics of these flow alignments, but in ways that can to a degree be reproduced by the simpler models. In particular, the tensor alignments observed in the DNS are surprisingly similar on average to those from the uniform random sampling case in the inertial range, while in the dissipation range they are more similar to the random vector fields. We argue that this difference suggests that in the dissipation range, turbulence tends to exhibit alignments sampled directly from the space of possible geometric configurations, while in the inertial range, it appears to sample from the space of rotation operators instead. Perhaps most intriguingly, we also find that the embedding dimension plays a very strong role in setting the behavior of the scale-to-scale energy flux. In particular, when we project the alignment into the space of 2D configurations, we see net inverse energy transfer regardless of the dynamics, consistent with

the expected inverse energy cascade in 2D turbulence. This finding suggests that the inverse cascade in 2D turbulence may be largely kinematic, which could offer an explanation for its observed lack of intermittency [24] (and indeed the conjectured lack of intermittency for all 2D cascades [25]). Taken together, these results present alternative ways of thinking about scale-to-scale energy transfer in turbulence and suggest potentially fruitful directions for turbulence modeling.

We begin in Sec. II by setting out the theoretical background for our study and describing our data sets. In Sec. III we present the results of our work: that the alignment between the turbulent stress and strain rate plays a larger role in the cascade than their magnitudes, that these alignments are determined partially by the flow dynamics, and that inverse energy flux generically results from projecting into 2D configurations. Finally, in Sec. IV we discuss and contextualize the implications of these results.

II. BACKGROUND AND METHODOLOGY

A. Defining scale-to-scale flux

The origin of the coupling between scales in fluid flow is the quadratic nonlinearity in the Navier-Stokes equations. This scale coupling is evident in the wave-vector triads that appear when the equations are transformed into Fourier space [26], but also has a signature in physical space. The application of any linear operator $\mathcal{P}$ that projects away some of the degrees of freedom of the flow to the momentum equation results in the appearance of the quantity [21]

$$\tilde{\tau}_{ij} = \mathcal{P}(u_i u_j) - \mathcal{P}(u_i)\mathcal{P}(u_j), \tag{1}$$

where u_i is the velocity and the tilde denotes a quantity defined for the projected flow so that, for example, $\mathcal{P}(u_i) \equiv \tilde{u}_i$. $\tilde{\tau}_{ij}$ plays the role of a stress, as its divergence appears as a source term in the momentum equation. Depending on the exact form of the projector $\mathcal{P}$, $\tilde{\tau}_{ij}$ goes by different names; for example, if $\mathcal{P}$ is a Reynolds averaging operator, $\tilde{\tau}_{ij}$ is a Reynolds stress, while if $\mathcal{P}$ is a low-pass filter deeper in the inertial range, $\tilde{\tau}_{ij}$ is a subgrid stress. Here we will generically refer to $\tilde{\tau}_{ij}$ as a turbulent stress, since its form does not depend on the details of $\mathcal{P}$. As detailed below, we will take $\mathcal{P}$ to be a low-pass filter, but will vary the filter scale.

This turbulent stress also appears in the energy equation for the projected field [27–29], most notably in the term

$$\tilde{\Pi} = -\tilde{\tau}_{ij}\tilde{s}_{ij}, \tag{2}$$

where $\tilde{s}_{ij} = (1/2)(\partial\tilde{u}_i/\partial x_j + \partial\tilde{u}_j/\partial x_i)$ is the rate of strain of the projected field. Note that, in incompressible flow, $\tilde{s}_{ii} = 0$; thus, the trace of the stress tensor, which does *not* in general vanish, does not contribute to $\tilde{\Pi}$. In the following, we will therefore always make the stress tensor deviatoric by removing its trace. This $\tilde{\Pi}$ term appears as a source or sink in the energy equation and physically represents the transfer of energy between scales. We will refer to $\tilde{\Pi}$ as the spectral energy flux; note that $\tilde{\Pi} > 0$ means a flux of energy to smaller scales (i.e., forward cascade), and $\tilde{\Pi} < 0$ means a flux of energy to larger scales (i.e., inverse cascade). Although this term is the physical-space analog of the usual triad interactions, it takes the form of a mechanical work term—that is, the action of a stress (arising from the degrees of freedom that have been projected away) against a rate of strain. In this way, the energy cascade can be interpreted as the result of some scales doing work on others and thereby transferring their energy.

Both the form of Eq. (2) and its interpretation as a mechanical work term, however, imply that the relative alignment of the turbulent stress and strain rate is essential for determining whether energy is actually transferred between scales: Regardless of the magnitude of each of these two tensors, if they are orthogonal to each other then $\tilde{\Pi} = 0$. Previously, we studied the geometric properties of the alignment of these tensors in turbulence [21]. In three dimensions, quantifying this alignment requires choosing a representation of the 3D rotation group SO(3); here we choose to use the ZXZ Euler angles ϕ, θ, and ψ. For convenience, we here absorb the negative sign in Eq. (2) into the stress $\tilde{\tau}_{ij}$ so that we study the alignment between the negative stress and the strain rate. Let us label

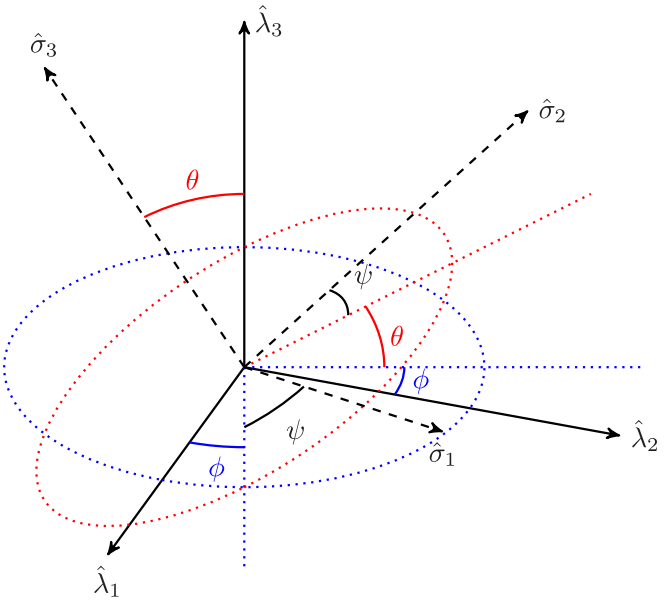

FIG. 1. Sketch of the eigenframes of the stress and strain rate and the ZXZ Euler angles used to move between the two. Transforming from the eigenbasis of the stress to the strain rate corresponds to a rotation by ϕ around $\hat{\boldsymbol{\lambda}}_3$, a rotation by θ about the rotated $\hat{\boldsymbol{\lambda}}_1$, and finally a rotation by ψ about the rotated $\hat{\boldsymbol{\lambda}}_3$.

the (unit) eigenvectors of $-\tilde{\tau}_{ij}$ as $\hat{\boldsymbol{\lambda}}_\alpha$ (where $\alpha \in \{1, 2, 3\}$) and of $\tilde{s}_{ij}$ as $\hat{\boldsymbol{\sigma}}_\alpha$. Transforming from the eigenbasis of the stress to the strain rate then corresponds to a rotation by ϕ around $\hat{\boldsymbol{\lambda}}_3$, a rotation by θ about the rotated $\hat{\boldsymbol{\lambda}}_1$, and finally a rotation by ψ about the rotated $\hat{\boldsymbol{\lambda}}_3$. A sketch of how this sequence of operations is applied is given in Fig. 1. Note that these Euler angles (and the associated coordinate system) are local, in that they map between the eigenframes of the stress and strain rate, which vary spatially in the flow field. If we additionally label the eigenvalues of the stress as $\lambda_1 > \lambda_2 > \lambda_3$ and of the strain rate as $\sigma_1 > \sigma_2 > \sigma_3$, we can write the spectral energy flux as [21]

$$\begin{aligned}\tilde{\Pi} = {} & \lambda_1\sigma_1[(1+\cos^2\theta)\cos 2\psi\cos 2\phi - 2\cos\theta\sin 2\phi\sin 2\psi] \\ & + \lambda_3\sigma_3[(1+\cos^2\theta)(1+\cos^2\phi)(1+\cos^2\psi) - 3(\cos^2\psi+\cos^2\phi) - \tfrac{1}{2}\cos\theta\sin 2\phi\sin 2\psi] \\ & + \lambda_1\sigma_3\{\cos 2\phi[(1+\cos^2\theta)(1+\cos^2\psi) - 3] - \cos\theta\sin 2\phi\sin 2\psi\} \\ & + \lambda_3\sigma_1\{\cos 2\psi[(1+\cos^2\theta)(1+\cos^2\phi) - 3] - \cos\theta\sin 2\phi\sin 2\psi\}, \end{aligned} \tag{3}$$

where we have used the incompressibility condition to eliminate the intermediate eigenvalues. This expression is quite complex, but its two most salient features for our purposes are that (a) it cannot be factored into a part depending only on the eigenvalues and a part depending only on the alignment of the eigenframes and (b) it cannot vanish due to misalignment alone [21]. Both of these aspects are different from the 2D case, where we only need to consider a representation of SO(2). In that case, the spectral energy flux *does* factor and can be fully suppressed only by alignment [22,30]. Thus, in three dimensions, both the eigenvalues and the Euler angles are in principle necessary to determine the flux of energy between scales.

An additional key difference between three and two dimensions becomes apparent when we make the distinction between a geometric configuration of the stress and strain rate (that is, the particular directions of the eigenvectors of the two tensors in space) and the rotation operator (or, equivalently, set of Euler angles) that one must apply to move from the eigenbasis of one tensor to the other. In both three and two dimensions, each geometric configuration is unique. In two dimensions, there is

a one-to-one mapping between the value of the single Euler angle and each unique configuration. However, in three dimensions, some geometric configurations can be achieved by many different Euler-angle triplets, each one an independent element of SO(3). We will return to this point below.

Finally, we note that just because it cannot be suppressed fully by misalignment alone does not mean that the energy flux is always large. To quantify the amount of energy transferred between scales relative to the maximum amount possible, we recently introduced the notion of an efficiency for the cascade [21,22]. We define this efficiency as

$$\Gamma = \frac{\tilde{\Pi}(\lambda_\alpha, \sigma_\alpha, \phi, \theta, \psi)}{\max_{\phi,\theta,\psi}[\mathrm{sgn}(\tilde{\Pi})\tilde{\Pi}(\lambda_\alpha, \sigma_\alpha, \phi, \theta, \psi)]}. \tag{4}$$

The numerator of this expression is the actual energy flux that occurs, while the denominator is the maximum possible energy flux for the same flow conditions given optimal choices for the Euler angles. Because of the sign term in the denominator, $\Gamma > 0$ means that the flux is in the same direction (in a spectral sense, that is, to larger or smaller scales) as the maximum possible flux, while $\Gamma < 0$ means that it is in the opposite direction. The denominator of Γ cannot in general be computed *a priori*, so in practice we evaluate it by simply numerically optimizing Eq. (3) given a particular set of eigenvalues. As we have reported before, Γ is on average not very large; for both 3D and 2D turbulence, $\langle\Gamma\rangle \approx 20$–$25\,\%$ in the inertial range [21,22], where the angular brackets denote an average over space and time.

B. Data sets

To explore the relative contributions of tensor magnitude, eigenframe alignment, flow dynamics, and geometric constraints on the scale-to-scale energy flux, we analyzed three different data sets: a DNS of forced homogeneous isotropic turbulence, an ensemble of random, multiscale solenoidal vector fields, and simple Monte Carlo sampling from uniform distributions of the relevant parameters in Eq. (3).

The DNS data were obtained from the Johns Hopkins Turbulence Database (JHTDB). Details of the simulation are given on the JHTDB website and are reported in Ref. [31]. The Navier-Stokes equations were solved using a pseudospectral algorithm on a 1024^3 grid in a triply periodic domain, achieving a Taylor-microscale Reynolds number of $R_\lambda = 433$.

The random vector fields were constructed similarly to those used in kinematic simulation [23]. We specified these fields on the same 1024^3 grid as used for the DNS. A number of different scales of motion were defined ranging from the grid spacing up to the domain size and separated algebraically (that is, linearly spaced between the minimum and maximum values). For each scale, a vector field was defined via a collection of Fourier modes with random phases and directions, with the imposed constraint of incompressibility. The total energy of the flow was apportioned between scales following a Kolmogorov $k^{-5/3}$ energy spectrum. The final velocity field was then obtained by summing over all the scale-local fields, after which it was treated just as if it had come from the DNS. An ensemble of such fields was generated. Due to the way they were constructed, the spatial correlation length of each random field is finite, but each member of the ensemble is uncorrelated with the other members.

Random sampling was done simply by choosing uniformly distributed values from the appropriate ranges for the relevant variables in Eq. (3): ϕ, θ, ψ, λ_1, λ_3, σ_1, and σ_3. The eigenvalues were sampled ensuring that λ_1 and σ_1 were greater than zero, λ_3 and σ_3 were less than zero, and their values could correctly generate deviatoric tensors with possible choices for the intermediate eigenvalues. Given that an overall factor of $\lambda_3\sigma_3$ can be scaled out of our calculations [comparing Eqs. (3) and (4)], this amounted to choosing $\lambda_3 = \sigma_3 = -1$ and allowing λ_1 and σ_1 to vary between $1/2$ and 2.

In all cases, we used 1024^3 samples per scale to compute statistics for eigenvalues and Euler angles. We determined statistical convergence empirically, by subsampling the data sets to see when

distributions no longer changed as more data were added. Convergence was typically attained for order 10×1024^2 samples.

Finally, we note that for both the random vector field and uniform random sampling cases, we do not expect any actual scale-to-scale energy flux, since these synthetic fields have no dynamics. However, we can still discuss the geometric alignment properties between τ_{ij} and s_{ij}, which are both still definable, and will tend to describe these alignments in terms of the flux they would produce if the two tensors had dynamical importance.

C. Flux calculation

Actually computing energy fluxes requires us to specify the operation $\mathcal{P}$ that projects away some of the degrees of freedom of the flow. As we are interested in the energy cascade and the directed flux of energy between scales, we define it to be a low-pass filter, conceptually similar to what is used in large-eddy simulation. This filtering approach allows us to specify the spectral energy flux in a spatiotemporally resolved way, as has been extensively documented in previous work [20,27–29,32–35]. Specifically, we define the filtered velocity field to be

$$\mathcal{P}(u_i) = \tilde{u}_i(\mathbf{x}) = \int G_r(\mathbf{x} - \mathbf{x}')u_i(\mathbf{x}')d\mathbf{x}', \tag{5}$$

where G_r is a filter kernel that suppresses components of the velocity field with spatial scales smaller than r. The detailed form of G_r does not strongly influence our results [21,28,30,36]; thus, for convenience, we take G_r to be the product of a sharp spectral filter (that is, a step function in Fourier space) multiplied by a sine function with a small bandwidth to avoid ringing. We implement this operation numerically on the simulation grid. Though this simple filter may not be the best choice for large-eddy simulation (LES) due to realizability considerations [37], it is satisfactory for our purposes in that it simply separates the effects of large and small scales. Prior studies have found that the use of a sharp spectral filter is not likely to change nature of the results for the type of geometric analysis we investigate here [38–40].

With this choice of $\mathcal{P}$, $\tilde{\Pi}$ should properly be interpreted as the flux of energy between all of the retained larger spatial scales of the turbulent field and all of the suppressed smaller scales. However, given the local nature of the energy transfer in the cascade, most of the flux should be localized to interactions between the scales just larger than the filter scale r and those just smaller than it. This interpretation has been confirmed by previous studies using the filtering approach [40–42]. We also note that there is nothing in this definition that presupposes what direction the flux should go (that is, from large to small or small to large scales).

We compute $\tilde{\Pi}$ using this method for both the DNS and random vector fields. In each case, we can perform this for any filter scale r that is in the computed range of scales. For the case of randomly sampled angles and eigenvalues, we simply compute the flux $\tilde{\Pi}$ directly from the definition in Eq. (3).

III. RESULTS

A. Effects of tensor magnitude and alignment on scale-to-scale flux

As described above, both the eigenvalues of the turbulent stress and strain rate and the Euler angles that describe the relative alignment of the two eigenframes are in principle necessary to determine the spectral energy flux $\tilde{\Pi}$ and efficiency Γ, since the two are inextricably linked in Eq. (3). Empirically, however, we find that the angles play a much more significant role in setting these quantities than do the eigenvalues.

To test the relative importance of the eigenvalues and the angles, we computed the spatiotemporally averaged efficiency $\langle\Gamma\rangle$ for different combinations of Euler angles and eigenvalues drawn from our three different data sets. We did these calculations for many spatial scales ranging from the top of the dissipation range into the middle of the inertial range. As shown in Fig. 2, $\langle\Gamma\rangle$ is

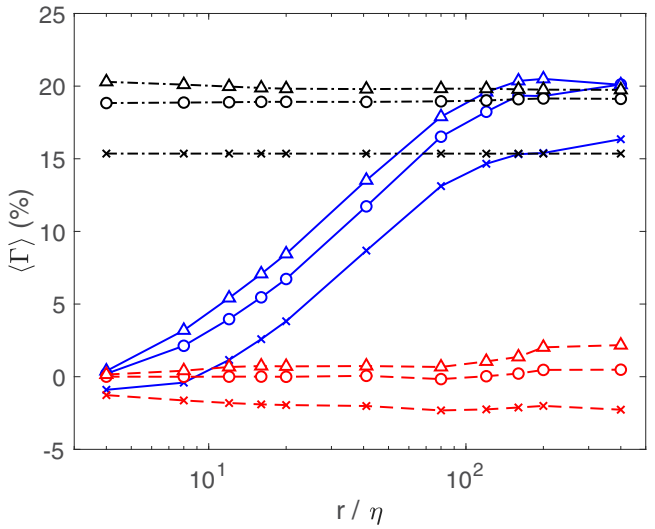

FIG. 2. Mean efficiencies $\langle\Gamma\rangle$ as a function of scale r/η for combinations of eigenvalues and Euler angles taken from different data sets. The line styles distinguish the data sets from which the angles were drawn. Data with blue solid lines correspond to angles taken from the DNS, with red dashed lines to angles taken from the random vector fields, and with black dash-dotted lines to uniformly sampled random angles. The symbols distinguish the data sets from which the eigenvalues were drawn. Triangles correspond to eigenvalues taken from the DNS, circles to eigenvalues taken from the random vector fields, and crosses to uniformly sampled random eigenvalues.

primarily set by the angles chosen: The three curves generated using angles taken from the DNS but eigenvalues from all three data sets are similar to each other but quite different from those with randomly sampled angles or angles taken from the random vector fields, which are themselves internally consistent but different from each other. Thus, it is clear that the eigenvalues play less of a role in setting the efficiency, and therefore the fundamental properties of the cascade, than the Euler angles do.

Even though there is a sense in which Γ normalizes out the eigenvalues, given that we optimize over the eigenframe alignment in Eq. (4), the result that the eigenvalues do not significantly determine Γ is not obvious, given the complexity of Eq. (3) and the fact that the eigenvalues cannot be factored out. Indeed, empirically, fixing the eigenframe alignment and varying the eigenvalues changes the efficiency aside from the special cases of eigenframe alignments that lead to $\Gamma = 100\%$ or -100%. These cases bear some additional discussion, as they reveal some of the purely geometric aspects of the cascade. Regardless of the eigenvalues, the minimum efficiency (that is, $\Gamma = -100\%$), occurs when the eigenvectors of the stress and strain rate corresponding to their largest (in magnitude) eigenvalues are perfectly antialigned—that is, when $\hat{\boldsymbol{\sigma}}_1$ points along $\hat{\boldsymbol{\lambda}}_3$, $\hat{\boldsymbol{\sigma}}_3$ points along $\hat{\boldsymbol{\lambda}}_1$, and $\hat{\boldsymbol{\sigma}}_2$ points along $\hat{\boldsymbol{\lambda}}_2$. This is the only configuration that will produce $\Gamma = -100\%$. As one would expect, the perfectly aligned case (that is, the case when $\hat{\boldsymbol{\sigma}}_\alpha$ points along $\hat{\boldsymbol{\lambda}}_\alpha$ for all α), leads to $\Gamma = 100\%$, the maximum value. However, although there is only a single set of Euler angles that produces the perfectly antialigned case (given by $\phi = \theta = \psi = \pi/2$), there are many sets of Euler angles that give the perfectly aligned case. For example, if $\theta = 0$, any choice of ϕ and ψ with $\phi = -\psi$ will lead to perfectly aligned eigenvectors and so will produce $\Gamma = 100\%$. Because there are more ways to sample the space of angles and achieve high efficiency than low efficiency in 3D space, there is an inherent and purely geometric bias toward forward energy flux in 3D turbulence.

The data in Fig. 2 for randomly sampled angles and random vector fields show little variation with scale, which makes sense since these fields have no dynamics, let alone scale-dependent dynamics.

The efficiency for the random vector fields is close to zero regardless of the eigenvalues chosen, which is to be expected since these fields are multiscale but uncorrelated across scales; thus, there is no reason to expect any net scale-to-scale energy flux or coupling of any kind. It is somewhat surprising, however, to see that uniformly sampling random angles *does* lead to configurations that would produce a nonzero scale-to-scale flux. We interpret this as further evidence of the geometric bias toward forward energy flux described above. Even more intriguingly, the DNS results essentially interpolate between the random vector field limit in the dissipation range to the random sampling limit in the inertial range. We can interpret this result by appealing to the expected turbulence dynamics. In the dissipation range, the local Reynolds number is less than unity, and so while the dissipation-range velocity fields are unsteady and may be spatiotemporally chaotic, they are no longer turbulent. In that limit, then, the flow field should be well approximated as a random vector field. At larger scales in the inertial range, however, the flow is more vigorous and the scale-local velocity fields are expected to be rough. Thus, in the inertial range the turbulent dynamics serve to scramble the Euler angles that map between the stress and strain-rate eigenframes, a process that is reasonably approximated by pure random sampling.

As a caveat, however, we note that Fig. 2 shows only the average efficiency. Even though the mean values for the DNS are well reproduced by uniform random sampling in the inertial range, the full distributions of efficiency may not be the same. To illustrate this point, in Fig. 3 we show the probability density functions (PDFs) of Γ for eigenvalues taken from the DNS and angles taken from the three different data sets at three different scales: $r/\eta = 8$, near the dissipation range; $r/\eta = 40$, in the transitional range of scales between the dissipation range and the inertial range; and $r/\eta = 200$, well into the inertial range. As expected given that the mean values are close to zero, the PDFs for the random vector fields are close to symmetric and peaked at $\Gamma = 0$. The PDFs for both the DNS and the uniform random sampling case are skewed toward positive values of Γ; however, even though the DNS PDF begins to approach that of the random sampling as r increases and has a similar mean value, it maintains a clearly different shape even in the inertial range. These findings augment the conclusion drawn in the preceding paragraph. The random vector fields appear to sample from the space of geometric configurations and thus show efficiency PDFs with no skewness, while the uniform random sampling case (by construction) samples instead from the space of Euler angles and shows highly skewed efficiency PDFs. Real turbulence falls somewhere between these two limiting cases, but is closer to sampling configurations at small dissipation-range scales and sampling Euler angles [or, equivalently, elements of SO(3)] at larger inertial-range scales.

Finally, we note that the PDFs of Γ for the random sampling cases have an additional and instructive interpretation that bolsters our discussion above of the inherent geometric bias toward positive efficiency in 3D space. These PDFs were constructed using the particular ensembles of eigenvalues found from the DNS but randomly sampling over the full ranges of possible Euler angles. Thus, each of these PDFs can be interpreted essentially as a density of states for the efficiency—that is, a representation of the number of different Euler-angle combinations that can produce a given efficiency given specified eigenvalues. As argued above, there is a clear and strong bias toward positive efficiency states purely given the geometric constraints. In contrast, this density of states in two dimensions is symmetric about $\Gamma = 0$, showing no bias.

B. Angle statistics

Given that the eigenvalues of the stress and the strain rate play only a secondary role in setting the character of the energy flux through the cascade, the differences between the three cases we have studied must primarily come from the eigenframe alignment. These angles are at least partially determined by the flow dynamics, as can be seen by studying their statistics.

First, we examined whether the three Euler angles were statistically independent by comparing their joint PDFs to the product of their marginal PDFs (not shown). In all cases, we found that the ratio of these quantities was close to unity everywhere, indicating statistical independence; thus, we

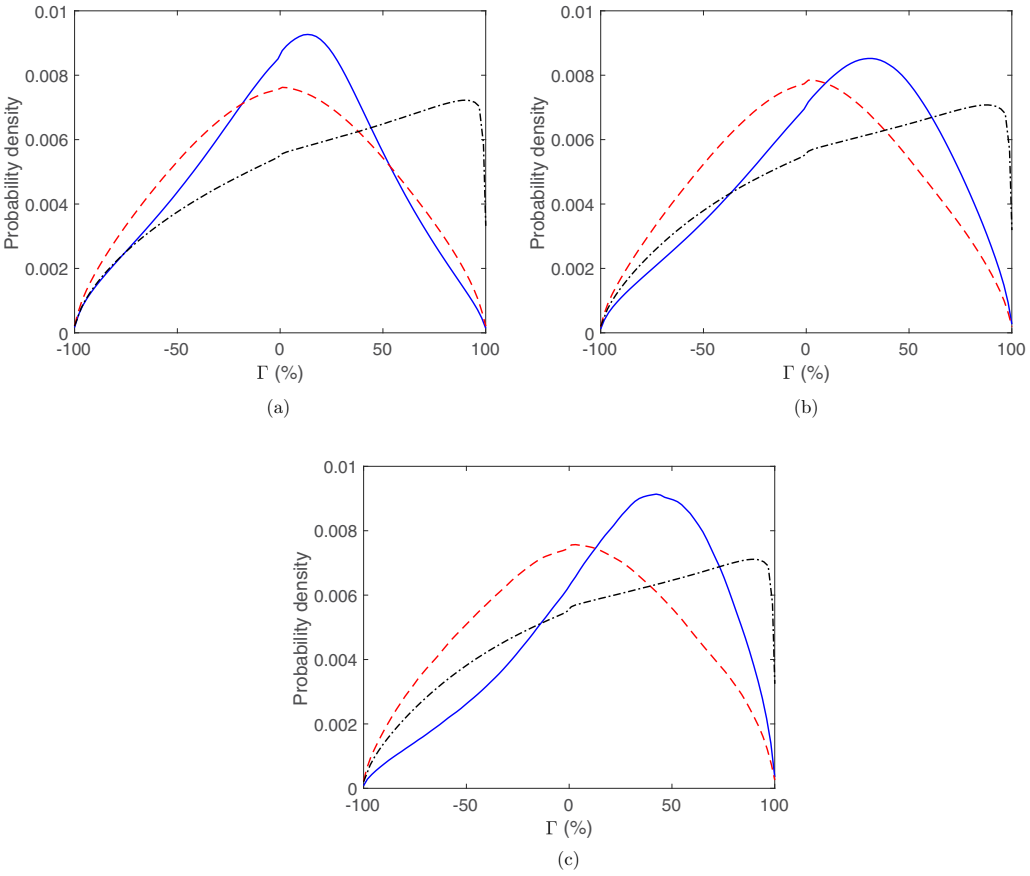

FIG. 3. Probability density functions of Γ for (a) $r/\eta = 8$, (b) $r/\eta = 40$, and (c) $r/\eta = 200$. All eigenvalues were taken from the DNS. As in Fig. 2, the line style shows the data set from which the angles were taken. Blue solid lines correspond to the DNS, red dashed lines to the random vector fields, and black dash-dotted lines to uniformly sampled random angles.

report here only the marginal PDFs of the three angles. In Fig. 4 we show these PDFs for both the DNS velocity fields and the random vector fields; our random angle case corresponds to choosing all these PDFs to be uniform (shown by the horizontal lines in Fig. 4). We note that, due to the symmetries that arise because we are considering eigenvectors that are essentially apolar, ϕ and ψ need only be considered on the interval $[0, \pi]$ and θ, as a polar angle, only on the interval $[0, \pi/2]$.

The PDFs for the DNS and the random vector fields are clearly different from each other and from the uniform case, supporting our conclusion that the dynamics of the flow play a role in setting the eigenframe alignments. At very small filter scales, the PDF of ϕ is similar for the DNS and the random vector field, showing a bimodal distribution with peaks at approximately $\pi/4$ and $3\pi/4$. This bimodal shape can qualitatively be understood by noting that, ϕ is constrained to lie between 0 and π and the efficiency tends to be lowest when $\phi = \pi/4$ or $3\pi/4$ [21]. In the dissipation range where Γ is small, then, we would expect the PDF of ϕ to be peaked at (at least) one of these values. Since there is no reason to expect one of them to be preferred over the other statistically, we see the observed bimodal shape.

This shape does not vary with scale for the random field, but does for the DNS. As the filter scale increases, the PDF of ϕ for the DNS case becomes unimodal and develops a peak at $\pi/2$, but as the filter scale increases further into the inertial range, the peak decays and the PDF approaches the

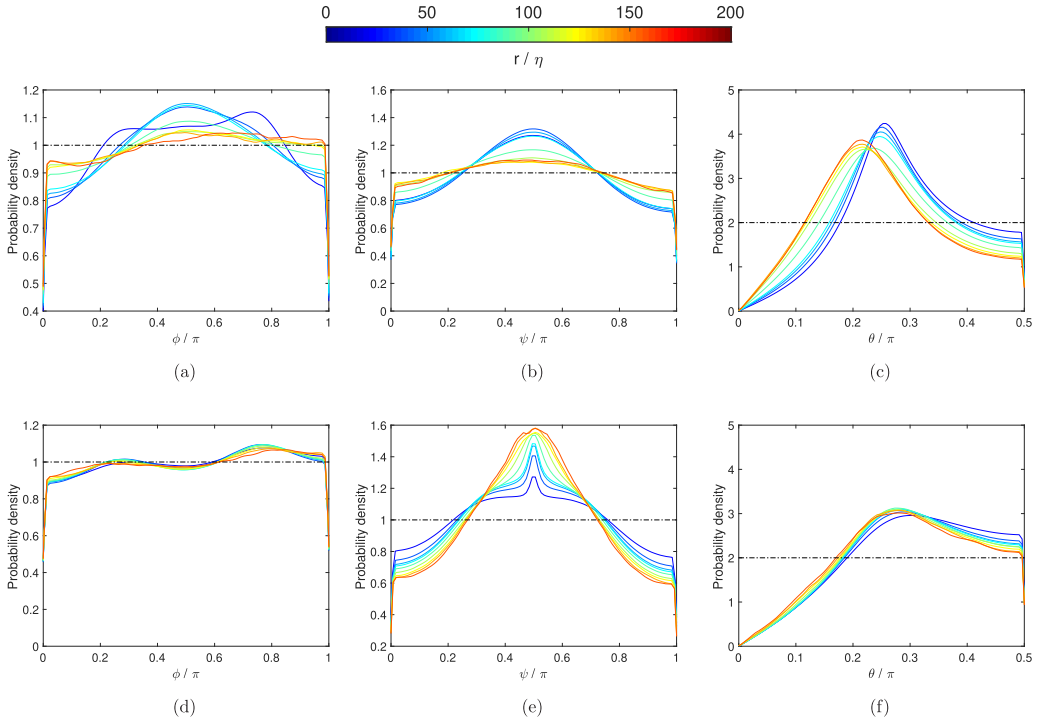

FIG. 4. Marginal PDFs of the Euler angles ϕ, ψ, and θ for (a)–(c) the DNS and (d)–(f) the random vector fields. Data are shown for $r/\eta = 8$, 12, 16, 20, 40, 80, 120, 160, and 200, as distinguished by color. The dash-dotted horizontal lines show the corresponding PDFs for the uniformly distributed case.

uniform case. This shift of the DNS data from being similar to the random field at small scales but closer to the uniform case at inertial-range scales (as observed above for the mean efficiency) is also apparent for ψ, where the PDF for the DNS data shows a peak at $\pi/2$ at small scales that relaxes as the filter scale increase. In contrast, this peak actually grows with filter scale for the random field case.

The PDFs for θ are somewhat different from those for ϕ and ψ, because for both the DNS and the random vector field they show a pronounced skewness toward $\theta > \pi/4$ at all scales, never relaxing to the uniform case. As we discuss further below, this skewness has significant consequences, as it can be tied to upscale energy transfer. As with the ϕ statistics, the PDF of θ is nearly independent of filter scale for the random vector field. For the DNS case, the skewness of the PDF and the position of the peak both decrease as the filter scale increases in the inertial range, shifting away from the random vector field result. At present, we do not have a detailed explanation for the shape of these PDFs; however, some simple tests implicate both the mathematical forms of the stress and strain rate, i.e., that the stress is constructed from the square of the velocity field and the strain rate from its gradient, and the incompressibility condition in setting the PDF shapes.

We note also that these results make it clear that the random solenoidal vector fields are random in the sense that the *phases* of the Fourier modes that make up the fields are random numbers, but this does not mean that the angles between the stress and strain rate are random. Rather, as is clear from Figs. 4(d)–4(f), the statistics of these angles are far from random and, indeed, far from the DNS results in the inertial range, which are in fact better represented as random. This finding is part of why a uniform angle approximation does a better job of reproducing $\langle\Gamma\rangle$ from the DNS than does the random vector field approximation (Fig. 2), though the residual nonuniformity of the angles, particularly for θ, leads to an incorrect PDF of Γ (Fig. 3).

C. Two-dimensional configurations

These results suggest that the polar Euler angle θ deserves a closer look to understand the role it plays in the scale-to-scale energy transfer. Thus, we would like to isolate only the θ dynamics out of our data sets. One way to accomplish this task would be to compute statistics of θ conditioned on ϕ and ψ taking particular specified values. Such an approach, however, would significantly decrease the size of the ensemble, leading to poorly converged statistics. Instead, we can take advantage of the near statistical independence of the three angles and simply set ϕ and ψ to whatever we wish (effectively replacing their PDFs with δ functions), but leave θ free. Physically, this can be thought of as projecting the full 3D structure of the eigenframe alignment problem down to two dimensions, where a single angle is sufficient to define the energy flux and the efficiency [22]. Given our definition of Euler angles, the most interpretable 2D projection is to set $\phi = \pi/2$ and $\psi = -\pi/2$ so that θ gives the angle of a pure rotation about the intermediate eigenvector of the stress [21]. With this choice, the energy flux defined in Eq. (3) reduces to

$$\tilde{\Pi}_\theta = [\lambda_1\sigma_1 + \lambda_3\sigma_3 - \lambda_1\sigma_3 - \lambda_3\sigma_1]\cos^2\theta + [\lambda_1\sigma_1 + \lambda_3\sigma_3 + 2\lambda_1\sigma_3 + 2\lambda_3\sigma_1]. \tag{6}$$

If this were true (incompressible) 2D turbulence, we would also have $\lambda_1 = -\lambda_3 = \lambda_{2D}$ and $\sigma_1 = -\sigma_3 = \sigma_{2D}$, leading to

$$\tilde{\Pi}_{2D} = 2\lambda_{2D}\sigma_{2D}\cos 2\theta, \tag{7}$$

the expected 2D turbulence result [22,35,43]. We note that the flux in the true 2D case factors into a part dependent only on the eigenvalues and a part dependent only on the eigenframe alignment, unlike in three dimensions. This factorization cannot be done, however, when we retain the eigenvalues from the full 3D dynamics.

As is well known, 2D turbulence shows on average an inverse cascade of energy, so that energy propagates spectrally from the scales at which it is injected into the flow to *larger* scales [44–46]. What is surprising is that we recover this result when we measure the efficiency computed using Eq. (4) but replacing the full energy flux $\tilde{\Pi}$ with the projected flux computed from Eq. (6). As shown in Fig. 5, $\langle\Gamma\rangle$ is either negative (signifying inverse energy flux) or close to zero regardless of the eigenvalues chosen and for values of θ taken from any of our data sets. Indeed, $\langle\Gamma\rangle$ is even more strongly negative when the angles are taken from the random fields and is zero for the randomly sampled angles, suggesting that (as expected) the geometric bias toward forward flux is not present in two dimensions. This result is consistent with the PDFs shown in Figs. 4(c) and 4(f), where the distributions of θ are clearly skewed toward values larger than $\pi/4$. When inserted into Eq. (7), noting that λ_{2D} and σ_{2D} are positive definite, $\theta > \pi/4$ makes $\tilde{\Pi}_{2D} < 0$, signifying inverse energy flux in 2D turbulence. Our findings show that this pattern holds in 3D turbulence as well, so regions of the flow where ϕ is close to $\pi/2$ and ψ is close to $-\pi/2$ will tend to have inverse energy transfer and thus will be regions of backscatter.

IV. DISCUSSION AND CONCLUSIONS

By writing the flux of energy between scales in turbulence as the inner product of the turbulent stress that accounts for the transfer of momentum between scales and the strain rate of the resolved scales, we have been able to study independently the roles of the magnitudes of these tensors in the turbulent cascade, as encoded by their eigenvalues, and the alignment between their eigenframes. As we argued, the sizes of the eigenvalues are determined almost completely by the dynamics of the flow, with their only constraint being that they need to sum to zero; however, the alignment between the eigenframes has strong geometric constraints due to the embedding dimension and the properties of the rotation group. In particular, we showed that these purely geometric properties impose a bias toward forward energy transfer in 3D space.

Mathematically, the energy flux is determined by both the eigenvalues of the stress and the strain rate and the alignment of their eigenframes in a complex way, since Eq. (3) does not factor. However, as we showed, the eigenvalues play a much less significant role in determining the behavior of

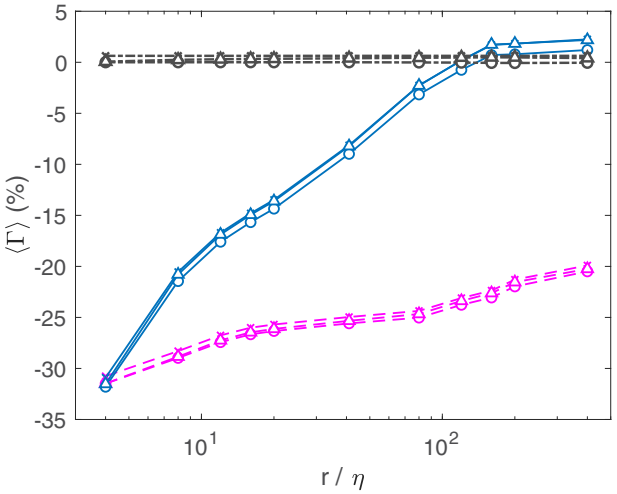

FIG. 5. Mean efficiency as a function of scale for combinations of eigenvalues and angles taken from different data sets, as in Fig. 2, but for the case of 2D configurations. As in Fig. 2, the line styles show the data sets from which the angles were taken: Solid lines correspond to (projected) angles from the DNS, dashed lines to the random vector fields, and black dash-dotted lines to uniformly sampled random angles. Symbols show the data sets from which the eigenvalues were taken. Triangles correspond to eigenvalues taken from the DNS, circles to eigenvalues taken from the random vector fields, and crosses to uniformly sampled random eigenvalues.

the flux, since swapping the eigenvalues in one data set with those from another changes the efficiency by only a small amount compared to the difference in efficiency found for the different eigenframe alignments. Thus, although it cannot be shown analytically since Eq. (3) does not factor, the character of the flux is determined primarily by the eigenframe alignment and not the magnitude of the tensors involved, and thus is essentially a kinematic quantity once the Euler angles have been specified. This finding suggests surprisingly that the well known patchy spatial distribution of the local energy flux, which is often implicated as a cause of intermittency, may not be linked to the heavy tails in the distributions of the magnitudes of the stress and strain rate, but rather to something else.

The kinematic nature of how the character of the flux is determined by the Euler angles is bolstered by our finding that projecting the alignment into two-dimensional configurations generically leads to inverse energy flux regardless of the eigenvalues or the flow dynamics: When the tensors are aligned and moving in essentially a 2D fashion, energy is transferred upscale. This result is conceptually similar to the recent demonstration that some mode triads with particular senses of helicity always show inverse transfer even in 3D turbulence [47]. The kinematic nature of this inverse flux is also intriguing given that inverse cascades are widely thought to be nonintermittent [25], whereas direct cascades clearly can be. Such a lack of intermittency could potentially arise from a lack of dynamics driving inverse energy flux, as opposed to direct flux. This conjecture would be interesting to investigate in future work.

It would also be interesting to use the ideas and framework we have described here to study anisotropic or inhomogeneous turbulence. The presence of the wall in a channel flow or a boundary layer, for example, breaks symmetries and has been shown to modify the alignment between the turbulence stress and strain rates [48].

Finally, our results here are suggestive of some potentially fruitful directions to take in turbulence modeling. Standard Smagorinsky-type LES models assume that the turbulent stress and strain rate are perfectly aligned but scale the magnitude of one relative to the other via an eddy viscosity. Our results point toward a wholly different strategy for closing the filtered equations of motion,

since the eigenframe alignment appears to play a more important role than the tensor magnitudes. On average, the simple assumption of random alignment with uniformly distributed Euler angles does a reasonable job of replicating the mean efficiency found in the DNS, given that (empirically) turbulence appears to sample elements of SO(3) rather than geometric configurations in the inertial range; it would be interesting to see how well an LES closure that makes this assumption would perform.

ACKNOWLEDGMENT

This research was supported by the US National Science Foundation under Grant No. CBET-1706950.

[1] A. N. Kolmogorov, The local structure of turbulence in incompressible viscous fluid for very large Reynolds numbers, Dokl. Akad. Nauk SSSR **30**, 301 (1941).
[2] R. Benzi, G. Paladin, G. Parisi, and A. Vulpiani, On the multifractal nature of fully developed turbulence and chaotic systems, J. Phys. A: Math. Gen. **17**, 3521 (1984).
[3] G. Parisi and U. Frisch, in *Turbulence and Predictability in Geophysical Fluid Dynamics*, Proceedings of the International School of Physics "E. Fermi," Course LXXXVIII, Varenna, 1985, edited by M. Ghil, R. Benzi, and G. Parisi (North-Holland, Amsterdam, 1985), p. 84.
[4] U. Frisch, *Turbulence: The Legacy of A. N. Kolmogorov* (Cambridge University Press, Cambridge, 1995).
[5] A. Arnèodo *et al.*, Structure functions in turbulence, in various flow configurations, at Reynolds numbers between 30 and 5000, using extended self-similarity, Europhys. Lett. **34**, 411 (1996).
[6] A. Arnèodo *et al.*, Universal Intermittent Properties of Particle Trajectories in Highly Turbulent Flows, Phys. Rev. Lett. **100**, 254504 (2008).
[7] G. I. Taylor, The transport of vorticity and heat through fluids in turbulent motion, Proc. R. Soc. London Ser. A **135**, 685 (1932).
[8] G. I. Taylor, Production and dissipation of vorticity in a turbulent fluid, Proc. R. Soc. London Ser. A **164**, 15 (1938).
[9] H. Tennekes and J. L. Lumley, *A First Course in Turbulence* (MIT Press, Cambridge, 1972).
[10] H. Xu, A. Pumir, and E. Bodenschatz, The pirouette effect in turbulent flows, Nat. Phys. **7**, 709 (2011).
[11] R. Ni, N. T. Ouellette, and G. A. Voth, Alignment of vorticity and rods with Lagrangian fluid stretching in turbulence, J. Fluid Mech. **743**, R3 (2014).
[12] W. T. Ashurst, A. R. Kerstein, R. M. Kerr, and C. H. Gibson, Alignment of vorticity and scalar gradient with strain rate in simulated Navier-Stokes turbulence, Phys. Fluids **30**, 2343 (1987).
[13] A. Tsinober, E. Kit, and T. Dracos, Experimental investigation of the field of velocity gradients in turbulent flows, J. Fluid Mech. **242**, 169 (1992).
[14] A. Vincent and M. Meneguzzi, The dynamics of vorticity tubes in homogeneous turbulence, J. Fluid Mech. **258**, 245 (1994).
[15] V. Borue and S. A. Orszag, Local energy flux and subgrid-scale statistics in three-dimensional turbulence, J. Fluid Mech. **366**, 1 (1998).
[16] R. Ni, S. Kramel, N. T. Ouellette, and G. A. Voth, Measurements of the coupling between the tumbling of rods and the velocity gradient tensor in turbulence, J. Fluid Mech. **766**, 202 (2015).
[17] A. Tsinober, Is concentrated vorticity that important?, Eur. J. Mech. B **17**, 421 (1998).
[18] M. Carbone and A. D. Bragg, Is vortex stretching the main cause of the turbulent energy cascade?, J. Fluid Mech. **883**, R2 (2020).
[19] S. Cerutti and C. Meneveau, Intermittency and relative scaling of subgrid-scale energy dissipation in isotropic turbulence, Phys. Fluids **10**, 928 (1998).
[20] S. Chen, R. E. Ecke, G. L. Eyink, M. Rivera, M. Wan, and Z. Xiao, Physical Mechanism of the Two-Dimensional Inverse Energy Cascade, Phys. Rev. Lett. **96**, 084502 (2006).

[21] J. G. Ballouz and N. T. Ouellette, Tensor geometry in the turbulent cascade, J. Fluid Mech. **835**, 1048 (2018).
[22] L. Fang and N. T. Ouellette, Advection and the Efficiency of Spectral Energy Transfer in Two-Dimensional Turbulence, Phys. Rev. Lett. **117**, 104501 (2016).
[23] J. C. H. Fung and J. C. Vassilicos, Two-particle dispersion in turbulentlike flows, Phys. Rev. E **57**, 1677 (1998).
[24] G. Boffetta and R. E. Ecke, Two-dimensional turbulence, Annu. Rev. Fluid Mech. **44**, 427 (2012).
[25] G. Falkovich, Symmetries of the turbulent state, J. Phys. A: Math. Theor. **42**, 123001 (2009).
[26] S. B. Pope, *Turbulent Flows* (Cambridge University Press, Cambridge, 2000).
[27] G. L. Eyink, Local energy flux and the refined similarity hypothesis, J. Stat. Phys. **78**, 335 (1995).
[28] M. K. Rivera, W. B. Daniel, S. Y. Chen, and R. E. Ecke, Energy and Enstrophy Transfer in Decaying Two-Dimensional Turbulence, Phys. Rev. Lett. **90**, 104502 (2003).
[29] Y. Liao and N. T. Ouellette, Spatial structure of spectral transport in two-dimensional flow, J. Fluid Mech. **725**, 281 (2013).
[30] Y. Liao and N. T. Ouellette, Long-range ordering of turbulent stresses in two-dimensional flow, Phys. Rev. E **91**, 063004 (2015).
[31] Y. Li, E. Perlman, M. Wan, Y. Yang, C. Meneveau, R. Burns, S. Chen, A. Szalay, and G. Eyink, A public turbulence database cluster and applications to study Lagrangian evolution of velocity increments in turbulence, J. Turbul. **9**, 31 (2008).
[32] M. Germano, Turbulence: The filtering approach, J. Fluid Mech. **238**, 325 (1992).
[33] S. Liu, C. Meneveau, and J. Katz, On the properties of similarity subgrid-scale models as deduced from measurements in a turbulent jet, J. Fluid Mech. **275**, 83 (1994).
[34] S. Chen, R. E. Ecke, G. L. Eyink, X. Wang, and Z. Xiao, Physical Mechanism of the Two-Dimensional Enstrophy Cascade, Phys. Rev. Lett. **91**, 214501 (2003).
[35] Y. Liao and N. T. Ouellette, Geometry of scale-to-scale energy and enstrophy transport in two-dimensional flow, Phys. Fluids **26**, 045103 (2014).
[36] D. H. Kelley and N. T. Ouellette, Spatiotemporal persistence of spectral fluxes in two-dimensional weak turbulence, Phys. Fluids **23**, 115101 (2011).
[37] B. Vreman, B. Geurts, and H. Kuerten, Realizability conditions for the turbulent stress tensor in large-eddy simulation, J. Fluid Mech. **278**, 351 (1994).
[38] J. A. Domaradzki and D. Carati, A comparison of spectral sharp and smooth filters in the analysis of nonlinear interactions and energy transfer in turbulence, Phys. Fluids **19**, 085111 (2007).
[39] J. A. Domaradzki and D. Carati, An analysis of the energy transfer and the locality of nonlinear interactions in turbulence, Phys. Fluids **19**, 085112 (2007).
[40] H. Aluie and G. L. Eyink, Localness of energy cascade in hydrodynamic turbulence. II. Sharp spectral filter, Phys. Fluids **21**, 115108 (2009).
[41] G. L. Eyink, Locality of turbulent cascades, Physica D **207**, 91 (2005).
[42] G. L. Eyink and H. Aluie, Localness of energy cascade in hydrodynamic turbulence. I. Smooth coarse graining, Phys. Fluids **21**, 115107 (2009).
[43] Z. Xiao, M. Wan, S. Chen, and G. L. Eyink, Physical mechanism the inverse energy cascade of two-dimensional turbulence: A numerical approach, J. Fluid Mech. **619**, 1 (2009).
[44] R. H. Kraichnan, Inertial ranges in two-dimensional turbulence, Phys. Fluids **10**, 1417 (1967).
[45] C. E. Leith, Diffusion approximation for two-dimensional turbulence, Phys. Fluids **11**, 671 (1967).
[46] G. K. Batchelor, Computation of the energy spectrum in homogeneous two-dimensional turbulence, Phys. Fluids **12**, 11233 (1969).
[47] L. Biferale, S. Musacchio, and F. Toschi, Inverse Energy Cascade in Three-Dimensional Isotropic Turbulence, Phys. Rev. Lett. **108**, 164501 (2012).
[48] C. W. Higgins, M. B. Parlange, and C. Meneveau, Alignment trends of velocity gradients and subgrid-scale fluxes in the turbulence atmospheric boundary layer, Bound.-Layer Meteorol. **109**, 59 (2003).